scientific reports

Check for updates

OPEN

Hepatic lipid metabolism is altered in *Ubiad1*$^{+/-}$ mice of both sexes

Ryoko Higa[1,2], Shirin Pourteymour[1], Pratibha S. Kolan[1], Simon N. Dankel[3,4], Johan Fernø[3,4], Gunnar Mellgren[3,4], Calvin Pan[5,6], Marcus M. Seldin[7], Aldons J. Lusis[5,6], Christian A. Drevon[1,8], Knut T. Dalen[1] & Frode A. Norheim[1]✉

UbiA prenyltransferase domain containing 1 (*Ubiad1*) has the potential to affect cholesterol and phospholipid levels in different cell types. We previously identified *Ubiad1* as a candidate gene for regulating subcutaneous fat pad weight in a mouse genome-wide association study. Here we evaluated the relationship between *Ubiad1* and obesity-related traits in cohorts of humans and mice, and in *Ubiad1*$^{+/-}$ mice fed a high-fat diet. In both humans and mice, adipose tissue *Ubiad1* mRNA expression correlated negatively with adiposity and positively with mitochondria-related genes. To determine the role of Ubiad1 in high-fat diet-induced obesity, we disrupted the *Ubiad1* gene in mice. Deletion of *Ubiad1* was embryonically lethal in C57BL/6 N mice, preventing analysis of adult *Ubiad1*$^{-/-}$ mice. Thus, male and female *Ubiad1*$^{+/+}$ and *Ubiad1*$^{+/-}$ mice were fed high-fat diet for 10 weeks, with no difference in weight gain and adipose tissue organ weights observed between the genotypes. Analysis of liver mRNA expression revealed that *Ubiad1* heterozygosis (*Ubiad1*$^{+/-}$) altered several pathways involved in lipid metabolism. Detailed lipid quantification with HPLC-qTOF/MS showed increased levels of hepatic ceramides in female *Ubiad1*$^{+/-}$ mice, whereas phosphatidylglycerols, phosohatidylinositol and lysophosphatidylethanolamines were reduced in male *Ubiad1*$^{+/-}$ mice. Our findings reveal sex-specific effects of *Ubiad1* expression on hepatic lipid metabolism.

Keywords NAFLD, Ubiad1, Sex differences, Lipid metabolism, RNA-seq, HPLC-qTOF/MS

Abbreviations

ERAD	ER-associated degradation
HFD	High-fat diet
HF/HS	High-fat and high-sucrose
HMDP	Hybrid Mouse Diversity Panel
HMGCR	HMG-CoA reductase
NAFLD	Non-alcoholic fatty liver disease
Ubiad1	UbiA prenyltransferase domain containing 1
CoQ-10	Coenzyme Q10
GWAS	Genome-wide association study
SVF	Stromal vascular fraction

The prevalence of obesity (body mass index (BMI) ≥ 30) is increasing at an alarming rate in both Europe and the US[1-3]. Obesity is strongly heritable in humans and mice, with estimates ranging from 50% to 90%[4,5]. Consumption of energy-dense diets rich in fat and refined carbohydrates and a sedentary lifestyle, are the key environmental contributors to the current obesity epidemic[6]. The obesity epidemic is associated with a rise in several cardiometabolic diseases, including type 2 diabetes, coronary heart disease, and non-alcoholic fatty

[1]Department of Nutrition, Institute of Basic Medical Sciences, Faculty of Medicine, University of Oslo, Sognsvannsveien 9, Domus Medica, 0372 Oslo, Norway. [2]Department of Medicine, New York University Grossman School of Medicine, New York, NY, USA. [3]Hormone Laboratory, Department of Medical Biochemistry and Pharmacology, Haukeland University Hospital, Bergen, Norway. [4]Mohn Center for Diabetes Precision Medicine, Department of Clinical Science, University of Bergen, Bergen, Norway. [5]Department of Medicine, Division of Cardiology, University of California, 650 Charles E Young Drive South, Los Angeles, Los Angeles, CA 90095, USA. [6]Departments of Human Genetics & Microbiology, Immunology, and Molecular Genetics, University of California, los Angeles, 650 Charles E. Young Drive South, Los Angeles, CA 90095, USA. [7]Department of Biological Chemistry, University of California, Irvine, Irvine, USA. [8]Vitas AS, Science Park, Gaustadalléen 21, 0349 Oslo, Norge. ✉email: f.a.norheim@medisin.uio.no

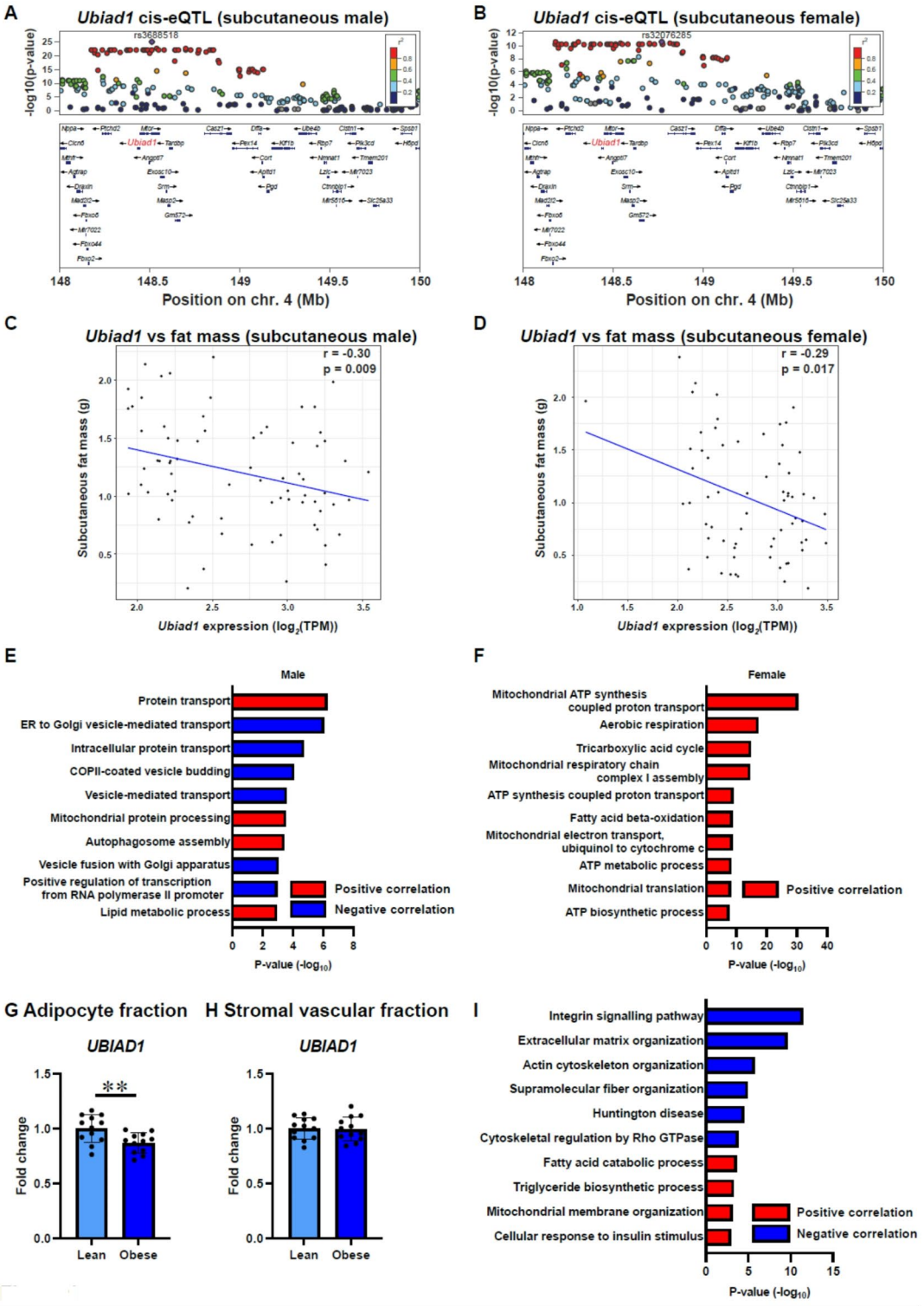

liver disease (NAFLD)[7-9]. NAFLD affects two billion adults globally, whereof 20% of these cases are expected to develop into non-alcoholic steatohepatitis[10,11].

Sex differences in body fat distribution and susceptibility to obesity, NAFLD, and other cardio-metabolic traits, have been described in both mice and humans, and are driven by genes as well as sex hormones[8,12–15]. Premenopausal females typically have greater subcutaneous fat depositions, whereas males and postmenopausal females tend to accumulate more visceral fat[12]. Studies on the menopausal transition in mice and humans, suggest that estrogen may increase energy expenditure and adipose tissue mitochondrial function[12,13]. The genetic contribution to body fat distribution have been shown in large-scale genome-wide association studies (GWAS) identifying several sex dimorphic loci[13,16].

We have previously identified an area on chromosome 4 exhibiting a genome-wide significant association with diet-induced subcutaneous fat accumulation in ~100 inbred male mice, but not in female mice or

◀**Fig. 1**. *Ubiad1* expression associates with subcutaneous adipose tissue weight. (**A**, **B**) Locus plot showing the associations between single nucleotide polymorphisms (SNPs) and subcutaneous adipose tissue *Ubiad1* expression on chromosome 4 in (**A**) male and (**B**) female HMDP mice. The significant associations between SNPs and *Ubiad1* mRNA expression levels in subcutaneous white adipose tissue (WAT) are depicted as dots and refer to the p-value of the association ($-\log_{10}$ of p-value), and location on chromosome 4. (**C**, **D**) *Ubiad1* mRNA expression is significantly correlated with subcutaneous WAT mass in (**C**) male and (**D**) female mice. (**E**,**F**) Pathway enrichment analysis using the top 500 genes that were strongest correlated with *Ubiad1* mRNA expression levels in the HMDP of (**E**) male, and (**F**) female mice. GO Biological process (GO BP) pathways were performed with positively correlated mRNAs (red) and negatively correlated mRNAs (blue) individually. The top 10 enriched pathways are presented. X-axis: P-value (-log10) of enriched terms. (**G**, **H**) Fold changes of *UBIAD1* mRNA expression in the (**G**) adipocyte fraction and (**H**) stromal vascular fraction (SVF) of subcutaneous WAT of lean or obese human subjects. *UBIAD1* mRNA was measured by Illumina microarrays. Data were normalized against the average *UBIAD1* expression of lean individuals. Data in graphs are shown as means ± SD (n = 12 per group). P-values were calculated with unpaired t test. **p < 0.01. (**I**) Pathway enrichment analysis of the mRNAs that correlated strongest (366 positively and 264 negatively correlated; correlation coefficient >0.6) with *UBIAD1* mRNA expression levels in adipocyte from subcutaneous WAT. PANTHER GO-Slim Biological Process pathway analyses[39] were performed individually with positively correlated mRNAs (red) and negatively correlated mRNAs (blue). The top 10 enriched pathways are presented. X-axis: p-value (-log10) of enriched terms.

humans[13]. One of the candidate genes in the identified region, which also has been implicated in regulation of lipid metabolism, was UbiA prenyltransferase domain containing 1 (*Ubiad1*)[13,17]. Ubiad1 is a transmembrane enzyme in the Golgi apparatus and the endoplasmic rectum (ER) membrane[18]. Ubiad1 catalyzes the conversion of phylloquinone-derived menadione (vitamin K_3) and forms the vitamin K subtype menaquinone-4 (MK-4)[19]. Loss of Ubiad1 reduces the cytosolic synthesis of coenzyme Q-10, which leads to increased reactive oxygen species-mediated lipid peroxidation in vascular cells[18]. Studies of Schnyder corneal dystrophy patients, a disease linked to a mutated *UBIAD1*gene, showed increased accumulation of cholesterol and phospholipids in the cornea[20,21]. This condition is characterized by the accumulation of crystals and lipids in the cornea, which can lead to blurred vision and reduced visual acuity. UBIAD1 enzymatic activities regulate ER-associated degradation (ERAD) of ubiquitinated HMG-CoA reductase (HMGCR)[22,23]. HMGCR is the rate-limiting enzyme of the mevalonate pathway that produces cholesterol and essential non-sterol isoprenoids. Accumulation of HMGCR due to mutated UBIAD1 leads to increased intracellular cholesterol in the cornea[22,23]. Unfortunately, whole body *Ubiad1*gene-deficiency in mouse seems to be embryonically lethal due to accelerated ER-associated degradation of HMGCR and dysregulated sterol synthesis[24], which complicates studies of the actual protein. We hypothesized that reducing Ubiad1 expression in mice would impact lipids associated with inflammation or cholesterol accumulation in obesity.

It is unclear if Ubiad1 affects diet-induced obesity, and it is not described in detail how Ubiad1 might affect accumulation of specific liver lipids in NAFLD. Thus, to evaluate the role of Ubiad1 in obesity and hepatic lipid metabolism, we associated adipose tissue *Ubiad1* expression with adiposity in cohorts of inbred mouse strains and humans, and investigated the role of Ubiad1 in heterozygous *Ubiad1* gene deficient mice (*Ubiad1*$^{+/-}$) fed a high-fat diet (HFD).

Results

Ubiad1 expression correlates negatively with adiposity in mice and humans

We previously identified a region on chromosome 4 that associated strongly with inguinal subcutaneous fat pad weight in ~100 male inbred strains fed a high fat/high sucrose (HF/HS) diet for 8 weeks[13]. The presence of a local expression quantitative trait locus (cis-eQTL) of a candidate gene, i.e., significant association of local single nucleotide polymorphism (SNP) with expression levels of that gene, would suggest that mRNA of this candidate gene could be a determinant of the trait. Our data indicate that adipose tissue *Ubiad1* expression show a strong cis-eQTL in both male (Fig. 1A) and female (Fig. 1B) mice. Furthermore, the subcutaneous adipose tissue *Ubiad1* mRNA level was negatively correlated with subcutaneous fat pad weight in male (Fig. 1C) and female (Fig. 1D) mice. We next used the DAVID GO bioinformatics resource[25,26] for enrichment analysis on the 500 adipose genes correlating most strongly with *Ubiad1* mRNA expression levels among the mice strains. The most significantly enriched pathways in male and female mice were protein transport (Fig. 1E) and mitochondrial respiration (Fig. 1F), respectively. Furthermore, Ubiad1 mRNA expression showed a positive association with expression of mitochondria-related genes in both sexes (Fig. 1E, F).

We followed up these findings in mice by investigating a bariatric surgery cohort to evaluate if the correlation between *UBIAD1* mRNA and obesity holds up in humans. *UBIAD1* mRNA in the adipocyte fraction of human subcutaneous adipose tissue was significantly reduced in obese individuals ($p = 0.0082$, Fig. 1G), supporting that *UBIAD1* expression levels are linked to body weight. We found no difference of the *UBIAD1* mRNA expression in the stromal vascular fraction of the subcutaneous adipose tissue between lean and obese individuals ($p = 0.93$, Fig. 1H), suggesting that fat content is correlated to *UBIAD1* mRNA expression in adipocytes but not adipose tissue stromal vascular cells. We next performed enrichment analysis with genes correlating the most strongly with *UBIAD1* mRNA levels in the adipocyte fraction of subcutaneous white adipose tissue (WAT). Using a correlation coefficient cut-off of more than 0.6, we identified 366 and 264 genes that correlated positively and negatively with *UBIAD1* expression, respectively. In accordance with the mice data (Fig. 1E, F), we observed

that expression of lipid- and mitochondria-related genes correlated positively with *UBIAD1* expression levels in human adipocytes (Fig. 1I).

Deletion of *Ubiad1* is embryonically lethal in C57BL/6 N mice

To investigate directly the role of Ubiad1 in obesity, we generated whole body knockout for *Ubiad1* in C57BL/6 N mice using CRISPR/Cas9 (Fig. 2A). Pairs of sgRNAs binding to the *Ubiad1* exon 1 were co-injected together with Cas9 RNA in embryos prior to implantation into foster mothers (Materials and Method). Among the generated founders, we identified an individual with a 29 bp deletion generating a frameshift resulting in a disrupted *Ubiad1* gene (Fig. 2A). Mating of heterozygous mice for the *Ubiad1* deletion ($Ubiad1^{+/-}$) produced only wild type ($Ubiad1^{+/+}$) and $Ubiad1^{+/-}$ offspring (Table 1), as observed by PCR analysis (Fig. 2B). In agreement with a previous report[24], we did not identify any $Ubiad1^{-/-}$ offspring, observed quite small litter sizes, and concluded that homozygous deletion of the *Ubaid* gene is embryonically lethal in the C57BL/6 N strain.

To be able to determine expression levels of mRNAs produced by the *Ubiad1* gene, we developed a two-pronged RT-qPCR assay. One component is designed specifically to detect only the wild-type *Ubiad1* mRNA (wt-transcript), whereas the other component is unable to distinguish between wild-type and the 29-bp mutated *Ubiad1* mRNAs (wt/null-transcripts). Whereas expression of wild type and mutated *Ubiad1* mRNAs was similar in $Ubiad1^{+/+}$ and $Ubiad1^{+/-}$ mice, expression of wild type *Ubiad1* mRNA was reduced ~ 50% in both subcutaneous WAT and liver of $Ubiad1^{+/-}$ mice (Fig. 2C, D). This suggests that the mutated $Ubiad1^{+/-}$ transcript is as stable as the wild type transcript, and that there is no compensating transcriptional regulation of *Ubiad1* mRNA expression in $Ubiad1^{+/-}$ mice. We next compared hepatic Ubiad1 protein levels between $Ubiad1^{+/+}$ and $Ubiad1^{+/-}$ mice using immunoblotting (Fig. 2E). We detected two bands in the predicted size range for the Ubiad1 protein (50 – 40 kDa). Whereas the strongest band at 50 kDa showed lower expression in $Ubiad1^{+/-}$ mice of both sexes, the 40 kDa showed similar expression between the genotypes in females.

Comparable body weight gains in $Ubiad1^{+/+}$ and $Ubiad1^{+/-}$ mice with HFD

We exposed $Ubiad1^{+/+}$ and $Ubiad1^{+/-}$ mice to a HFD and compared their weight gain after 10 weeks of diet intervention. All groups exhibited an increase in body weight and fat mass from the baseline due to the HFD (Fig. 3A-B). The relative weight gain in male $Ubiad1^{+/+}$ and $Ubiad1^{+/-}$ mice was 44.11 ± 19.09% and 46.08 ± 17.70%, respectively. Among female mice, the relative weight gain was 55.58 ± 21.40% in $Ubiad1^{+/+}$ and 49.51 ± 20.58% in $Ubiad1^{+/-}$. However, we observed no significant differences between the groups in terms of body weights (Fig. 3A), body compositions (Fig. 3B), liver weights (Fig. 3C), inguinal (Fig. 3D) and gonadal fat pad weights (Fig. 3E), or non-fasting plasma cholesterol levels (Fig. 3F) in either sex.

In accordance with unaltered adiposity, the expression of inguinal subcutaneous white adipose tissue mRNAs important for lipid metabolism was similar in $Ubiad1^{+/+}$ and $Ubiad1^{+/-}$ mice (Supplementary Fig. 1).

Increased expression of liver lipid-related genes in female $Ubiad1^{+/-}$ mice

Ubiad1 has been linked to Schnyder corneal dystrophy[27], a condition characterized by the progressive accumulation of cholesterol and lipids in the cornea. Disruption of the UBIAD1 enzyme's function leads to this abnormal accumulation, contributing to the disease's symptoms. Thus, we investigated the effect of reduced *Ubiad1* mRNA on the expression of genes relevant for hepatic lipid metabolism. Using qPCR, we found that mRNA expression levels of *Hmgcr* (Fig. 4A), *Ldlr* (Fig. 4B), *Pcsk9* (Fig. 4C), *Srebf2* (Fig. 4D), and *Pparg* (Fig. 4E) were elevated in livers of female $Ubiad1^{+/-}$ mice as compared to $Ubiad1^{+/+}$ mice. Although the mRNA expression of most of the genes showed similar trends in male and female mice, none of the mRNAs were significantly altered in male $Ubiad1^{+/-}$ mice (Fig. 4A-E). The expression of *Fasn* showed a tendency to be increased in $Ubiad1^{+/-}$ mice of both sexes (Fig. 4F).

Alterations in liver lipid metabolic pathways in $Ubiad1^{+/-}$ mice

To identify which mRNAs and pathways are influenced by reduced Ubiad1 expression, we conducted RNA sequencing to analyze global gene expression in the liver tissues of both male and female $Ubiad1^{+/+}$ and $Ubiad1^{+/-}$ mice. In livers of $Ubiad1^{+/-}$ males, 87 genes were increased, and 52 genes were decreased as compared to $Ubiad1^{+/+}$ (Fig. 5A and supplementary Table 1). In livers from female $Ubiad1^{+/-}$ mice, 68 mRNAs were significantly increased, whereas 16 mRNAs were reduced as compared to $Ubiad1^{+/+}$ mice (Fig. 5B and supplementary Table 2). Pathway analysis of the differently expressed genes between $Ubiad1^{+/-}$ and $Ubiad1^{+/+}$ showed significant effect on several pathways in both sexes (Fig. 5C, D). In particular, the pathways related to cholesterol biosynthesis, isoprenoid metabolism, farnesyl diphosphate metabolism, secondary alcohol biosynthesis, and sterol biosynthesis, were significantly enriched among the hepatic mRNAs that were increased in $Ubiad1^{+/-}$ as compared to $Ubiad1^{+/+}$ in male mice (Fig. 5C). In female $Ubiad1^{+/-}$ mice, lipid and triglyceride biosynthetic/metabolic processes were the most enriched up-regulated pathways (Fig. 5D). Overall, several hepatic lipid-related genes exhibited higher expression levels in $Ubiad1^{+/-}$ mice, leading to the upregulation of lipid metabolic pathways in both sexes.

Specific hepatic lipids are affected differently in male and female $Ubiad1^{+/-}$ mice

To determine if the observed differences in mRNA expression linked to lipid metabolism in $Ubiad1^{+/-}$ mice affected accumulation of lipids, we performed detailed lipid analysis with HPLC-qTOF/MS on the livers of $Ubiad1^{+/+}$ and $Ubiad1^{+/-}$ mice of both sexes (Fig. 6A-P and Supplementary Fig. 2).

Although female $Ubiad1^{+/-}$ mice exhibited enrichment of several lipid biosynthetic pathways (Fig. 5D), only liver ceramide levels were increased in $Ubiad1^{+/-}$ mice as compared to $Ubiad1^{+/+}$ mice (Fig. 6A). In livers from male $Ubiad1^{+/-}$ mice, PG (Fig. 6K), LPE (Fig. 6P), and PI (Fig. 6N) levels were decreased in $Ubiad1^{+/-}$ mice as compared to $Ubiad1^{+/+}$ mice. Conversely, levels of DAG (Fig. 6B) and FFA (Fig. 6L) tended to be higher in male

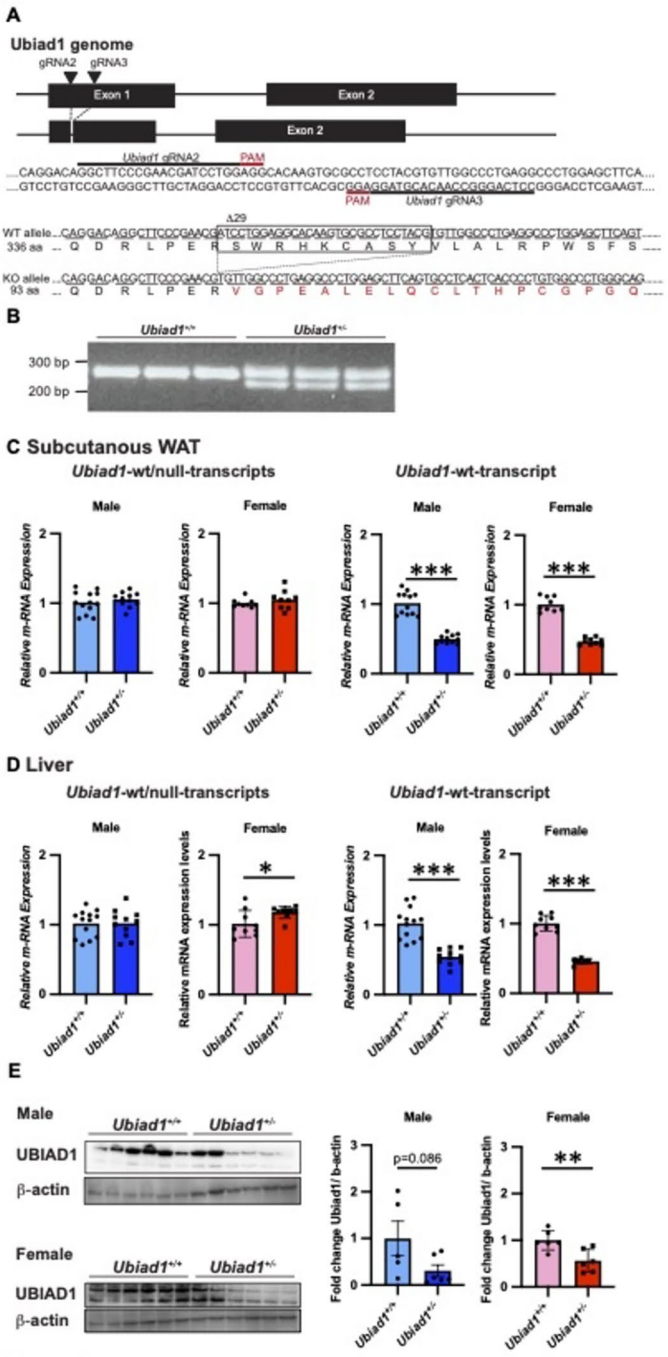

Fig. 2. Generation of *Ubiad1*$^{+/-}$ mice by the CRISPR Cas9 system. (**A**) A schematic drawing of the *Ubiad1* locus, binding sites for the two sgRNAs, and the generated disrupted *Ubiad1* allele. The 29 base pair deletion generating a frameshift mutation in the *Ubiad1* gene is marked on the WT allele. Amino acids marked with red color show the expected codon alterations generated due to the introduced frameshift mutation. (**B**) Migration of DNA fragments obtained with PCR amplification of a normal and mutated *Ubiad1* alleles. The predicted sizes of the DNA fragments are 265 bp for the *Ubiad1*$^{+/+}$ allele and 236 bp for the *Ubiad1*$^{+/-}$ allele. The gel image was cropped and original gels are presented in Supplementary Figure 5A. (**C**, **D**) Quantification of wild type and mutated *Ubiad1* mRNA transcripts, versus only wild type mRNA in (**C**) subcutaneous WAT and (**D**) liver in 20 weeks old mice fed HFD for 10 weeks. (n = 11–13 per group in males, n = 9 per group in females). Data were normalized against the expression of *Tbp* and *Rplp0*, respectively. (**E**) Western blot of Ubiad1 and beta-actin on whole liver proteins from *Ubiad1*$^{+/+}$ and *Ubiad1*$^{+/-}$ mice (n=6 per group). One sample from *Ubiad1*$^{+/+}$ male was excluded from the quantification analysis due to saturated band. The blots were cropped and original blots are presented in Supplementary Figure 5B. Data represent means ± SD. P-values were calculated using unpaired t-test. *p < 0.05, **p < 0.01, ***p< 0.001.

Number of offspring	*Ubiad1*$^{+/+}$	*Ubiad1*$^{+/-}$	*Ubiad1*$^{-/-}$	Total
***Ubiad1*$^{+/-}$x*Ubiad1*$^{+/-}$**				
Male	5	12	0	17
Female	11	13	0	24
Total	16	25	0	41
Average number of offspring per litter	2	3.1	0	5.1
Total number of breeding cages: 3				
Total number of breeding litters: 8				
***Ubiad1*$^{+/-}$x*Ubiad1*$^{+/+}$**				
Male	21	19	0	40
Female	22	24	0	46
Total	43	43	0	86
Average number of offspring per litter	4.3	4.3	0	8.6
Total number of breeding cages: 2				
Total number of breeding litters: 10				

Table 1. The number of offspring from the breeding of *Ubiad1*$^{+/-}$ X *Ubiad1*$^{+/-}$ or *Ubiad1*$^{+/+}$ X *Ubiad1*$^{+/-}$.

Ubiad1$^{+/-}$ mice, although this increase was not statistically significant ($p = 0.08$ and 0.06, respectively). Liver CE (Fig. 6O) levels were not significantly affected in *Ubiad1*$^{+/-}$ mice of either sex. Taken together, reduced Ubiad1 expression led to increased hepatic ceramide levels in females, whereas it decreased several phospholipids in males.

The fact that cholesterol storage was unaltered despite that several genes related to cholesterol biosynthesis were increased in the livers of *Ubiad1*$^{+/-}$ mice (Fig. 5C), suggests that compensating mechanisms contracts the altered gene expression in this lipid biosynthetic pathway of *Ubiad1*$^{+/-}$ mice. This is corroborated by Western blot analysis of membrane fractions from female livers, which show no significant differences between *Ubiad1*$^{+/-}$ and *Ubiad1*$^{+/+}$ mice in the cholesterol metabolism-related proteins Hmgcr, Ldlr, and Srebp2 (supplementary Fig. 4). Although the Srebp2 protein levels showed a slight tendency to increase in *Ubiad1*$^{+/-}$ mice, this trend corresponds with the levels of Srebp2 mRNA. Alternatively, extending the duration of the HFD intervention might be necessary to observe the impact of Ubiad1 on cholesterol accumulation and NAFLD in *Ubiad1*$^{+/-}$ mice. Combining extending the duration of the HFD intervention with histology, could reveal potential liver-related diseases caused by perturbed lipid accumulation.

Discussion

We have previously shown that *Ubiad1* reside in an area of chromosome 4 that has a genome-wide significant association with subcutaneous fat pad weight in male mice[13]. Here, we show that adipose tissue *Ubiad1* expression has a strong cis-eQTL in both male and female mice, and that its *Ubiad1* mRNA expression levels associate negatively with adiposity in both mice and humans. Studies on *Ubiad1*$^{+/-}$ mice fed a HFD revealed no effect on adiposity or subcutaneous fat pad weight but showed effects on mRNA transcripts of several liver lipid genes and sex-specific effects on accumulation of liver lipids. Each of these points are discussed below. Future research should explore the impact of Ubiad1 on traits related to insulin sensitivity.

Role of *Ubiad1* in obesity

The local genetic regulation of *Ubiad1* (cis-eQTL) and the associations between adipose tissue *Ubiad1* expression and adiposity in both mice and humans, support a role of Ubiad1 in development of obesity. This was further supported by a positive association between adipose tissue *Ubiad1* expression and expression of genes encoding mitochondrial synthesis and respiration (Fig. 1). On the other hand, the fact that we found no difference in adiposity or subcutaneous fat pad weight between *Ubiad1*$^{+/+}$ and *Ubiad1*$^{+/-}$ mice after HFD feeding for 10 weeks, suggests that a 50% reduction in *Ubiad1* mRNA expression is insufficient to cause an effect on obesity development. This is in line with a previous study reporting no difference in the total body weight of *Ubiad1*$^{+/+}$ and *Ubiad1*$^{+/-}$mice on a regular chow diet[24]. It is also possible that alternative genes or pathways may compensate for the reduced expression of Ubiad1 in *Ubiad1*$^{+/-}$ mice. For example, enzymes involved in cholesterol synthesis or lipid processing, such as HMG-CoA reductase or other prenyltransferases, might increase their activity to counterbalance diminished Ubiad1 function. This compensatory upregulation could obscure the complete effects of Ubiad1. It may also be necessary to extend the duration of dietary interventions to elucidate fully the role of Ubiad1 in lipid metabolism. Prolonged dietary regimens could increase metabolic stress, potentially unveiling more pronounced phenotypic differences and allowing for the observation of the long-term effects of Ubiad1 deficiency. Such studies would help determine whether the subtle changes currently observed are early indicators of more significant metabolic disturbances that take time to develop fully. Finally, other genes in the chromosome 4 locus might explain the subcutaneous fat pad association independent of Ubiad1. For example, adipocyte-specific deletion of the gene located next to *Ubiad1*, mechanistic target of rapamycin (*Mtor*, encoding the mTOR protein), has been suggested to inhibit adipose tissue development[28].

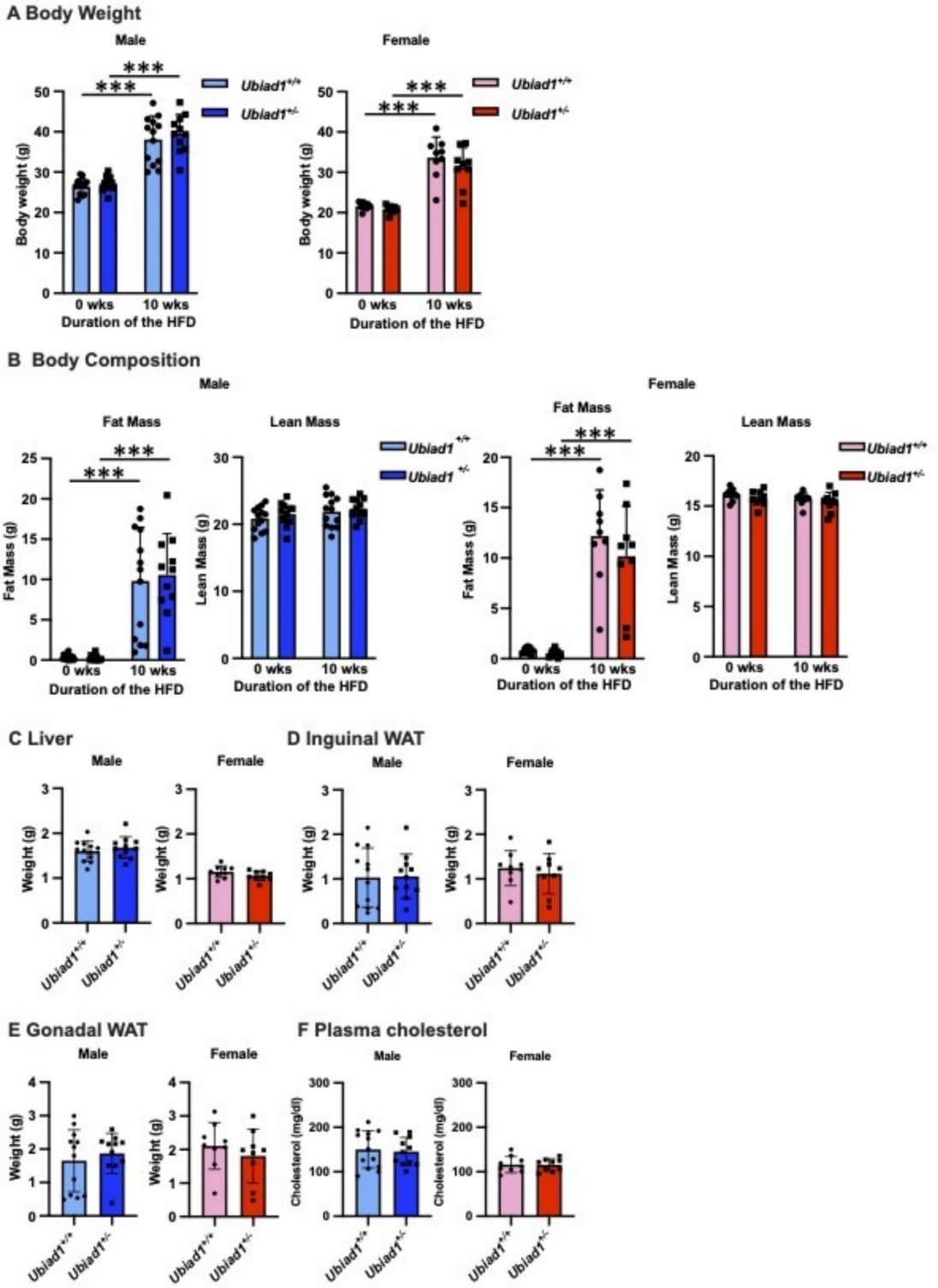

Fig. 3. No effect of lowered *Ubiad1*expression on obesity-related traits in mice on HFD. (**A**-**B**) (**A**) Total body weights and (**B**) body composition prior to (0 wks) and post (10 wks) HFD intervention in male and female *Ubiad1*$^{+/+}$ and *Ubiad1*$^{+/-}$ mice (n= 11–13 males, n = 9 females). (**C**-**E**) The weight of (**C**) liver, (**D**) inguinal WAT, and (**F**) plasma cholesterol levels at the end of the experiment. The mice were euthanized at 20 weeks of age in the morning (8–11 a.m.). Data represent means ± SD. P-values were calculated using Two-way ANOVA, with Fisher LSD test used for post-hoc multiple comparisons (A, B) or unpaired t test (C-F). ***p < 0.001.

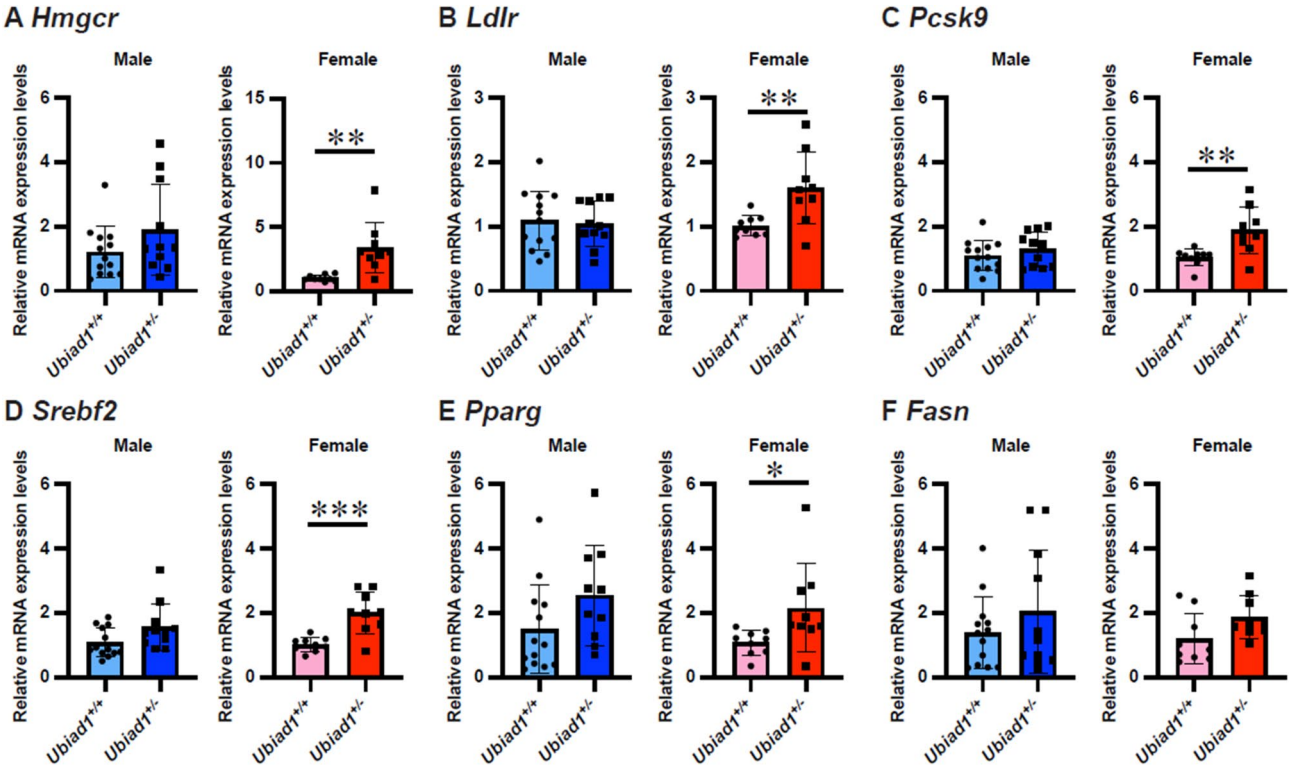

Fig. 4. The effect of *Ubiad1* mRNA expression on hepatic lipid metabolism. (**A-F**) Quantification of (**A**) *Hmgcr*, (**B**) *Ldlr*, (**C**) *Pcsk9*, (**D**) *Srebf2*, (**E**) *Pparg*, and (**F**) *Fasn* mRNAs in *Ubiad1*$^{+/+}$ and *Ubiad1*$^{+/-}$ livers of mice after 10 weeks of HFD. Data were normalized against *Rplp0* expression levels. Data represent means ± SD (n = 11–13 males, n = 9 females). P-values were calculated with unpaired t test. *p < 0.05, **p < 0.01, ***p < 0.001.

Sex-specific effect of *Ubiad1* in hepatic lipid accumulation

The Ubiad1 enzyme has several different functions including inhibition of ER-associated degradation of ubiquitinated HMGCR[22], and stimulation of menadione[19]and CoQ-10 synthesis[18]. Thus, we analyzed the effect of globally reduced Ubiad1 expression (*Ubiad1*$^{+/-}$) on hepatic mRNA expression, in particular lipid synthesis, using RNA sequencing in mice of both sexes. The number of altered mRNAs in *Ubiad1*$^{+/-}$ mice were higher in males than females (Fig. 5). However, in females, a larger proportion of the genes affected in *Ubiad1*$^{+/-}$ mice encoded proteins belonging to lipid metabolic pathways. Whereas cholesterol biosynthesis was the main pathway regulated in male *Ubiad1*$^{+/-}$ mice, lipid biosynthesis was the most regulated pathway in female *Ubiad1*$^{+/-}$ mice. Intriguingly, our detailed hepatic lipid quantification with HPLC-qTOF/MS showed that the lipid species altered in *Ubiad1*$^{+/-}$ mice also were different between the sexes. Whereas levels of LPE, PG, and PI were reduced in *Ubiad1*$^{+/-}$ male livers, ceramide levels were increased in *Ubiad1*$^{+/-}$females. Interestingly, a mouse line carrying Ubiad1 N100S point mutation with hyper-reflective dot-like deposits in the anterior cornea, show an increase in corneal PG without any changes in corneal cholesterol content[21]. Thus, Ubiad1 might have a stronger effect on accumulation of certain phospholipid species than cholesterol in livers of male mice. In theory, a reduction in Ubiad1 protein levels should lead to an accumulation of Hmgcr protein and cholesterol in the livers of *Ubiad1*$^{+/-}$ mice via ERAD-associated pathways. This would typically suggest a downregulation of *Hmgcr* transcript through feedback mechanisms. However, our findings in female *Ubiad1*$^{+/-}$ mice revealed decreased Ubiad1 protein levels, and unexpectedly showed increased *Hmgcr* mRNA levels (Figs. 4A and 5B) and no significant change in Hmgcr protein levels (supplementary Fig. 4) or liver CE (Fig. 6O). A previous study with a chow diet found slightly reduced Hmgcr protein levels in *Ubiad1*$^{+/-}$mice[24], aligning with our conclusion that HMGCR protein levels do not increase in these mice. The observed increase in Hmgcr transcription suggests a complex regulatory role of UBIAD1 in the liver, suggesting activation of positive feedback mechanisms.

We have previously shown a clear sex difference in the accumulation of hepatic ceramides and how they are regulated between the sexes[29]. The observed sex difference in hepatic ceramide levels was probably due in part to testosterone-mediated repression of the ceramide synthase 6 (*Cers6*) gene in male mice[29]. Here, we show that the mRNA levels of Ubiad1 might affect hepatic ceramide levels in female mice but not in male mice. This may indicate a general trend of increased inflammation in the livers of female *Ubiad1*$^{+/-}$ mice compared to *Ubiad1*$^{+/+}$ mice (supplementary Table 2). Additionally, we observed higher mRNA expression levels of *Cers5* and interleukin-1b (*Il1b*) in the livers of Ubiad1$^{+/-}$ females using qPCR (supplementary Fig. 3), with RNA sequencing data showing increased expression for *Il1b* only (supplementary Table 2). Increased ceramide levels in female *Ubiad1*$^{+/-}$mice could potentially lead to hepatic insulin resistance with prolonged HFD intervention[30].

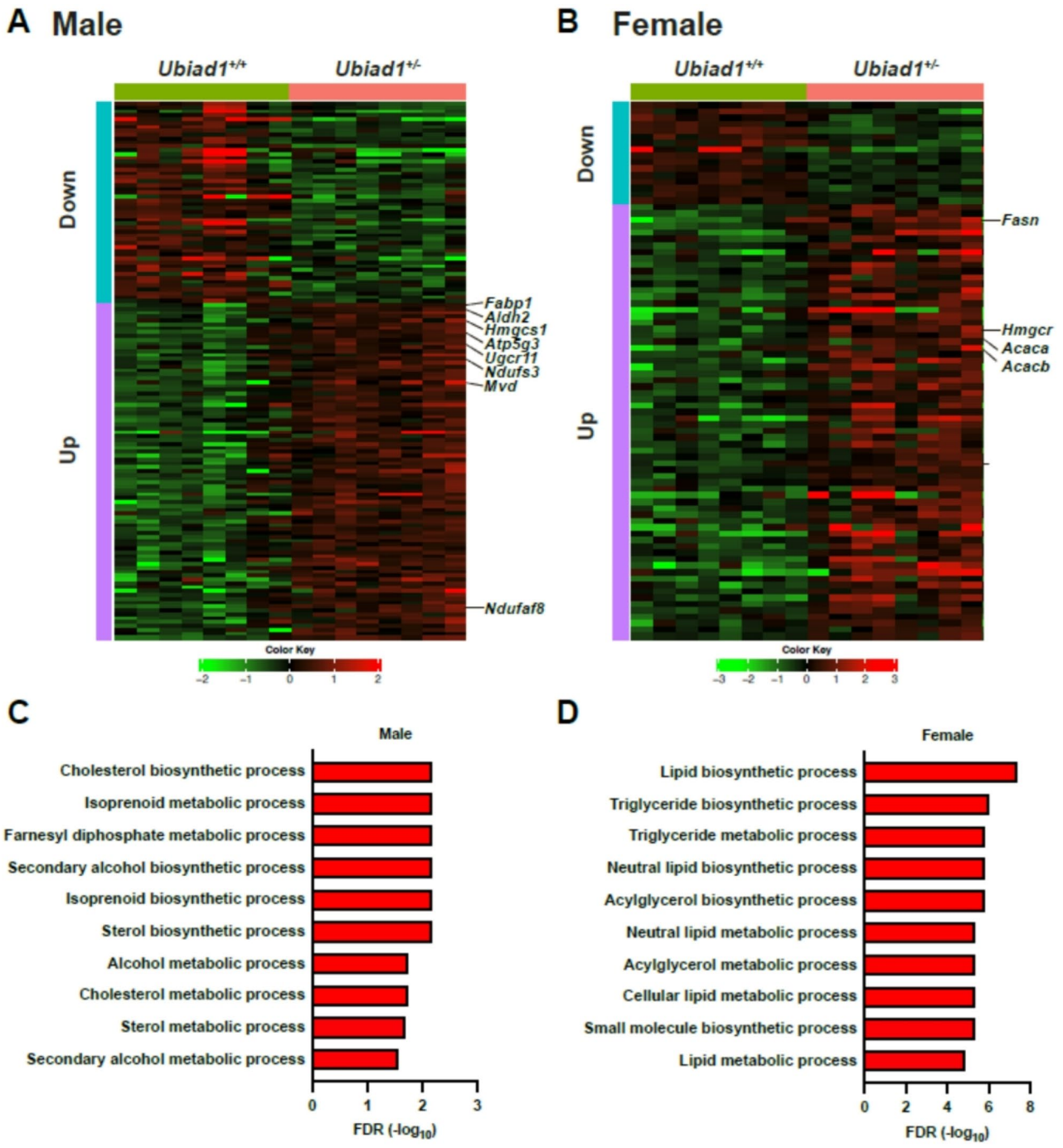

Fig. 5. Lower *Ubiad1* mRNA expression affects lipid biosynthetic pathways in male and female mice. (**A**,**B**) Heatmap of differentially expressed hepatic genes in *Ubiad1*$^{+/+}$ compared to *Ubiad1*$^{+/-}$ (**A**) male and (**B**) female mice (n = 8 per group) as determined by RNA sequencing (FDR < 0.05, FC > 1.5). (**C**, **D**) The 10 most significantly different hepatic mRNA expression pathways between *Ubiad1*$^{+/+}$ and *Ubiad1*$^{+/-}$ (**C**) male and (**D**) female mice, identified by enrichment analysis. The GO biological process pathway analysis was performed with differentially expressed genes. All the top 10 enriched pathways were increased in *Ubiad1*$^{+/-}$ mice.

Taken together, we have demonstrated significant effects on lipid-related genes in both male and female *Ubiad1*$^{+/-}$ mice for the first time. Notably, female *Ubiad1*$^{+/-}$ mice exhibited increased hepatic ceramide levels, whereas PG, PI, and LPE levels were reduced in male *Ubiad1*$^{+/-}$ mice. Extending the duration of a HFD feeding could uncover the potential clinical implications for fatty liver-related diseases. Future research should also explore the molecular mechanisms underlying the sex-specific role of Ubiad1 in hepatic lipid metabolism.

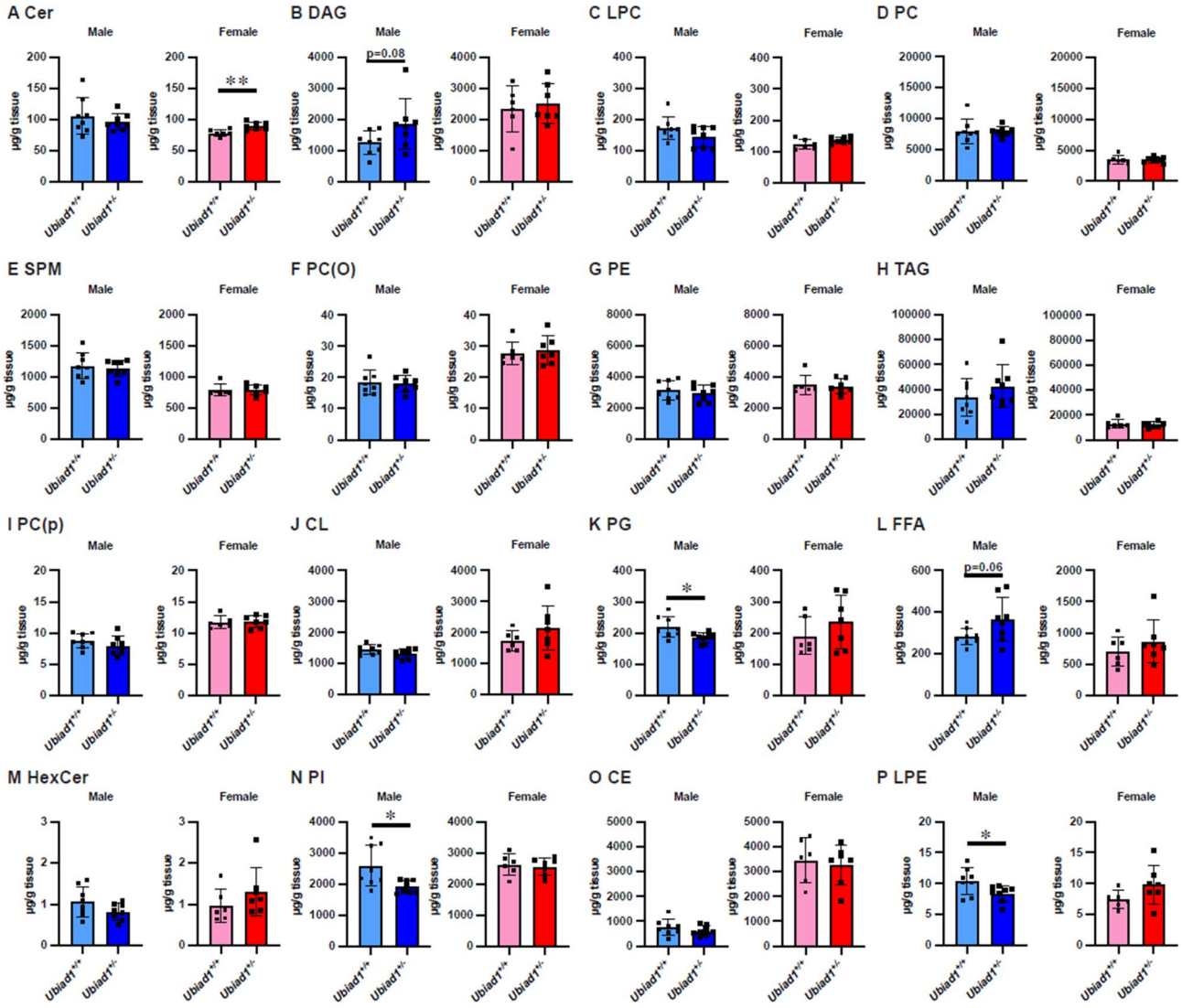

Fig. 6. Sex differences in hepatic lipid species with altered *Ubiad1* mRNA expression (**A-Q**). Concentration of (**A**) Cer, (**B**) DAG, (**C**) LPC, (**D**) PC, (**E**) SPM, (**F**) PC(O), (**G**) PE, (**H**) TAG, (**I**) PC(p), (**J**) CL, (**K**) PG, (**L**) FFA, (**M**) HexCer, (**N**) PI, (**O**) CE, and (**P**) LPE in the liver of male and female *Ubiad1*$^{+/+}$ and *Ubiad1*$^{+/-}$ mice fed HFD for 10 weeks. Data represent means ± SD (n = 8 males; n = 6–7 females). p-values were calculated with unpaired t test. *p < 0.05, **p < 0.01.

Conclusion

In conclusion, we have shown that *Ubiad1* expression in adipose tissue correlates with adiposity in both humans and mice, although there seems to be no difference in HFD-induced obesity between *Ubiad1*$^{+/+}$ and *Ubiad1*$^{+/-}$ mice. In livers of *Ubiad1*$^{+/-}$ mice, we observed increased expression of many cholesterol biosynthetic genes in male mice, and lipid biosynthetic genes in female mice. Detailed lipid quantification with HPLC-qTOF/MS analyses showed that hepatic ceramides were induced in female *Ubiad1*$^{+/-}$ mice, whereas several phospholipids were decreased in male *Ubiad1*$^{+/-}$ livers. These results suggest a sex-specific effect of *Ubaid1* in hepatic lipid metabolism.

Materials and methods

Human cohort

The human "ADIPO cohort"[31], comprising 12 lean individuals (mean ± SD BMI 22.8 ± 2.2 kg/m^2; weight 68.6 ± 10.9 kg; height 1.73 ± 0.10 m; age 43.5 ± 12.1 years) undergoing elective surgery and 12 individuals with obesity (mean ± SD BMI 43.7 ± 5.4 kg/m^2; weight 128.4 ± 16.1 kg; height 1.72 ± 0.11 m; age 43.1 ± 10.4 years) undergoing bariatric surgery, was approved by the Regional Ethics Committee in Western Norway (REC West, approval number 2018/2404). Each subject gave written informed consent before the start of the study, and the methods were carried out in accordance with relevant guidelines and regulations.

Adipocytes and stromal vascular fractions were obtained by digesting 700–800 mg of subcutaneous adipose tissue with collagenase and thermolysin (Liberase Blendzyme 3, Roche, Basel, Switzerland). The tissues were

cut into smaller pieces and digested in 4 mL of preheated Hanks' balanced salt solution with 2.6 Wunch units of Liberase Blendzyme 3 at 37 °C. After 30 min the samples were filtered through 25-mm and 200-mm mesh polypropylene filters (Spectrum Laboratories, Rancho Dominguez, CA, US). The filters were placed in an Easy Pressure syringe filter holder (PALL 4320, Life Sciences, Batavia, IL, US) and connected to a 10 mL Omnifix syringe (Braun Melsungen, Melsungen, Germany) to allow application of weak pressure. Following two rinses of the dissolved samples in Hanks' balanced salt solution/5% bovine serum albumin (A1311, US Biological, Swampscott, MA, US) and a few minutes time for floatation, the adipocytes were transferred to a 2 mL Eppendorf tube and rinsed once more. The non-floating cells were centrifuged at 400 g for 5 min and lysed in 1 mL Qiazol (Qiagen, Venlo, Netherlands), before freezing in liquid nitrogen and stored at − 80 °C. For gene expression analysis, RNA with high integrity was extracted from the adipocytes and stromal vascular fraction and converted to biotin-labeled cRNA, with subsequent hybridization of the cRNA to HumanHT-12v.3 Illumina Sentrix BeadChip microarrays before analysis in the Illumina iScan system (Illumina Inc., San Diego, CA, US).

Hybrid mouse diversity panel (HMDP)

The study was commenced in 2010. The use of animals and all experimental procedures were approved by the Institutional Care and Use Committee of the University of California, Los Angeles (UCLA) and conducted in accordance with the animal care guideline set by UCLA and the ARRIVE guidelines (https://arriveguidelines.org). The about 100 mouse strains from the HMDP panel included in the study, have been described in detail[5,13]. Briefly, male and female mice were maintained on a chow diet (Ralston Purina Co., MO, USA) until 8 weeks of age before switching to a HF/HS diet (#D12266B, Research Diet, NJ, USA) for 8 weeks. The macronutrient composition of the HF/HS diet was as follows: 16.8 E% from protein, 51.4 E% from carbohydrates, and 31.8 E% from fat. Mice were euthanized by cervical dislocation, and collected blood and tissues were snap frozen in liquid nitrogen. Subcutaneous (inguinal), mesenteric, gonadal, and retroperitoneal adipose tissues were weighed and flash-frozen in liquid nitrogen immediately after harvesting and stored at −80 °C. All mice were housed with a stable light/dark cycle (07 AM–07 PM), with 55 ± 5% relative humidity at 22 ± 2 °C in a specific pathogen-free animal unit.

Generation of *Ubiad1* deficient mice

All animal experiments in *Ubiad1* deficient mice were performed according to experimental procedures approved by the Norwegian Animal Research Authority (Mattilsynet, approvals FOTS id: #10902 and # 20822). Experiments conformed to the ARRIVE guidelines, Norwegian ethical guidelines (FOR-2015-06-18–761), and guidelines in the Directive 2010/63/EU of the European Parliament on the protection of animals used for scientific purposes. Mice were housed with 12 h light/dark cycle (07 AM to 07 PM), 55% relative humidity at 22 °C in a specific pathogen-free animal unit. Mice had free access to rodent chow (62 E% carbohydrate, 11 E% fat, 27 E% protein; #RM3A/SDS RM3, Scanbur, Denmark), and water. The presence of pathogens was monitored quarterly according to Federation of European Laboratory Animal Science Associations (FELASA) recommendations. Animals used in these experiments were specifically pathogen-free (SPF status) according to FELASA recommendations.

Ubiad1-deficient mice were generated at the Norwegian Transgenic center using CRISPR-Cas9 genome engineering[32]. The CRISPR Design tool was used to identify optimal guide RNA (gRNA) binding sites in the mouse *Ubiad1* gene (*Ubiad1* gRNA1: 5'-GGGACCCGCAGAAGAACGAA-3', *Ubiad1* gRNA2: 5'-GGCTTCCCGAACGATCCTGG-3', *Ubiad1* gRNA3: 5'-CCTCAGGGCCAACACGTAGG-3'). Oligoes corresponding to the above gRNAs (gRNA1-fw: 5'-CACCGGGACCCGCAGAAGAACGAA-3', gRNA1-rev: 5'-AAACTTCGTTCTTCTGCGGGTCCC-3', gRNA2-fw: 5'-CACCGGCTTCCCGAACGATCCTGG-3', gRNA2-rev: 5'-AAACCCAGGATCGTTCGGGAAGCC-3', gRNA3-fw: 5'-CACCGGCCTCAGGGCCAACACGTAGG-3', gRNA3-rev: 5'-AAACCCTACGTGTTGGCCCTGAGGCC-3') were phosphorylated by T4 polynucleotide kinase (New England Biolabs, MA, USA), annealed and cloned into a *BbsI*digested pX330 vector[32]. Cloned vectors were used as templates to PCR-amplify sRNAs with binding sites for T7 RNA polymerase (gRNA1-T4_fw: 5'-TTAATACGACTCACTATAGGGACCCGCAGAAGAACGAA-3', gRNA2-T4_fw: 5'-TTAATACGACTCACTATAGGCTTCCCGAACGATCCTGG-3', gRNA3-T4_fw: 5'-TTAATACGACTCACTATAGGCCTCAGGGCCAACACGTAGG-3', gRNA-T4_rev: 5'-AAAAGCACCGACTCGGTGCC-3'). The obtained PCR products were purified with agarose gel electrophoresis and used as templates for *in vitro* transcription of the gRNAs using the MEGAshortscript T7 Transcription Kit (#AM1354, Thermo Fisher, MA, USA).

Four weeks old female C57BL/6 N mice (Janvier Labs, Le-Genest-Saint-Isle, France) were super-ovulated (injection of 5 U PMSG followed by injection of 5 U hCG 45 h later), mated over night with C57BL/6 N male, and euthanized in the morning the following day to harvest fertilized 1-cell embryos. Cas9 mRNA (Sigma-Aldrich, St. Louis, MO, USA) and pairs of gRNAs were co-injected into embryos, followed by implantation of injected embryos into two pseudo-pregnant RjOrl: SWISS foster mothers (Janvier Labs, France). DNA extracted from ear biopsies of offspring was used to PCR amplify the targeted *Ubiad1* region (Ubiad1_fw; 5'-GCTTCCATGGCTGCGGTACA-3', Ubiad1_rev; 5'-CTGCACAACCCAACAACAGCCTG-3'). F0 founders carrying a mutated *Ubiad1* allele were identified by confirmation of heterogeneous DNA hybrids among amplified PCR products using heteroduplex DNA polyacrylamide gel electrophoresis. PCR fragments from promising founders were re-amplified with the following primers (5'-GGGGACAAGTTTGTACAAAAAAGCAGGCTGCTTCCATGGCTGCGGTACA-3' and 5'-GGGGACCACTTTGTACAAGAAAGCTGGGTCTGCACAACCCAACAACAGCCTG-3') and cloned into the Gateway pDONR 221 vector (Thermo Fisher, MA, USA). 10 individual clones from each founder were sequenced to characterize *Ubiad1* allelic variants in the founder. One F0 founder was identified with a 29 bp deletion as a result of double cleavage by gRNA2 and gRNA3 in the exon 1 of the *Ubiad1* gene. This 29 bp deletion was predicted to result in the production of a truncated, nonfunctional Ubiad1 protein. The F0 founder was mated to produce F1 offspring carrying the *Ubiad1*-deficient allele, and F1 offspring subsequently

Gene name	Forward primer	Reverse primer
Ubiad1-WT-allele	CAAGTGCGCCTCCTACGTG	GATCCAGGACACCCTGAGAC
Ubiad1-WT/null-allele	TCTCTACACAGGAGGAATTGGA	TGGACAGCGTAGGCAAACAT
Hmgcr	GCCTTGTGATTGGAGTTGGC	ACACTGACATGCAGCCGAAG
Ldlr	GACTGCAAGGACATGAGCGA	TGTCCAAGCTGATGCACTCC
Pcsk9	TGTCACAGAGTGGGACCTCA	CTCGGCCAGGGTAAGTGTG
Fasn	CTTCGGCTGCTGTTGGAAGTC	GTGTTCGTTCCTCGGAGTGAG
Pparg	TTGCTGTGGGGATGTCTCAC	AACAGCTTCTCCTTCTCGGC
Srebf1c	GGAGCCATGGATTGCACATTT	CAGCATAGGGGGCGTCAAA
Srebf2	TGACTCTCGGGGACATCGAC	CACCTCCAGGGAAGGAGCTA
Fabp4	GGGAACCTGGAAGCTTGTCTC	CCACTTTCCTTGTGGCAAAGC
Leptin	TGCTGCAGATAGCCAATGAC	GAGTAGAGTGAGGCTTCCAGGA
Adipoq	ATGGCAGAGATGGCACTCCT	CCTTCAGCTCCTGTCATTCCA
Plin1	ACCTGGAGGAAAAGATCCCG	TTCGAAGGCGGGTAGAGATG
Lpl	CGCTCTCAGATGCCCTACAA	CTGGTTGTGTTGCTTGCCAT
Scd1	GAGGCGAGCAACTGACTATC	GGTGGTCGTGTAAGAACTGG
Pdk4	AAGATGCTCTGCGACCAGTA	CAATGTGGATTGGTTGGCCTG
Cd68	CTCTAAGGCTACAGGCTGCTC	GACTGGTCACGGTTGCAAGA

Table 2. List of primer sequence for RT-qPCR.

back-crossed with C57BL/6 N mice for an additional generation to minimize the presence of possible off-target cleavages. The *Ubiad1* genotype was determined by PCR from ear tissue using the *Ubiad1*_fw and *Ubiad1*_rev primers (*Ubiad1* WT allele: 265 bp, *Ubiad1* KO allele: 236 bp).

Experimental animals were first generated by mating of heterozygous littermates ($Ubiad1^{+/}$). To determine if $Ubiad1^{-/-}$ mice were viable, three breeding cages with one male and two female $Ubiad1^{+/-}$ mice were arranged. Genotyping of obtained litters revealed no live $Ubiad1^{-/-}$ mice and reduced number of litters compared to the expected litter size (Table 2). After confirming the expected embryonal lethality[24], breeding cages were subsequently set up with $Ubiad1^{+/+}$ and $Ubiad1^{+/-}$ mice to generate animals for phenotypic analyses. Larger litter sizes were obtained from this heterozygous breeding (Table 2). A total of 23 male and 18 female *Ubiad1* littermates were produced to characterize the *Ubiad1*-deficient model in these studies.

Diet intervention and body composition

At 10 weeks of age, mice were fed a high-fat diet (HFD) with 60 E% from fat, 20 E% from carbohydrates, and 20 E% from protein (#D12492, Research Diet) for 10 weeks. Body weight and body composition were monitored at the start and the end of diet intervention using a Minispec LF90II TD-NMR machine (Bruker, Billerica, MA, USA). Mice were euthanized by cervical dislocation, and collected blood and tissues (liver, and perigonadal and inguinal subcutaneous white adipose tissue) were snap frozen in liquid nitrogen. A total of 41 mice were included in this study. No mice were excluded from the analyses, unless stated otherwise.

Reverse transcriptase quantitative PCR (RT-qPCR)

Liver and inguinal subcutaneous white adipose tissue (WAT) were homogenized in Qiazol reagent (Qiagen) by vigorous shaking with glass beads (Precellys 24, Bertin Technologies, Montigny-le-Bretonneux, France). Total RNA was subsequently isolated using a NucleoSpin RNA isolation kit (Macherey–Nagel, PA, USA), with a modified pre-preparation method[33]. RNA purity and concentration were measured on a NanoDrop ND-100 Spectrophotometer (Thermo Fisher Scientific, MA USA).

First strand cDNA was synthesized with random hexamers using a High-Capacity cDNA Reverse Transcription Kit (#4368814, Thermo Fisher Scientific) on an ep Gradient S Eppendorf Mastercycler (Eppendorf AG, Hamburg, Germany) with the following settings: 25 °C for 10 min, 37 °C for 120 min, 85 °C for 5 min and 4 °C on hold.

Real-time quantitative PCRs were performed with assay primers (200 nmol/L each) and Bio-Rad SsoAdvanced™ Universal SYBR® Green Supermix (10 µL reaction, 95 °C for 3 min, followed by 44 cycles of 95 °C for 10 s and 60 °C for 20 s) on a CFX96 Touch instrument (Bio-Rad, Hercules, CA, USA). Primers are listed in Table 2. Data were analyzed according to the ΔΔCt method, with normalization against mRNA expression of *Rplp0* (Liver) or *Tbp* (Subcutaneous WAT).

Immunoblotting

Liver was homogenized with lysis buffer (1% SDS, 10 mM Tris-HCl, 10 mM EDTA) containing complete Proteinase Inhibitor Cocktail (#11836170001, Roche) and phosphatase inhibitors (#P0044, Sigma-Aldrich) using glass beads (Precellys 24, Bertin Technologies). Samples were mixed with Leammeli buffer, heated at 95 °C for 5 min, and loaded into Criterion™ TGX™ 4–20% gels (Bio-Rad). Gels were transferred to Nitrocellulose using Trans-Blot Turbo RTA Transfer kit (Bio-Rad). Primary antibodies against rabbit anti-Ubiad1 (#ab191691, abcam, Waltham, MA, USA) and mouse anti-beta-actin (#A3854, Sigma-Aldrich).

Band intensities were quantified using Image Studio Software (LI-COR, Lincoln, NE, USA). Immunoblot signals were normalized to beta-actin levels.

RNA sequencing of liver

RNA sequencing of livers was performed as previously described[34]. Briefly, RNA integrity was determined using Bioanalyzer RNA 6000 Nano (Agilent Technologies, CA, USA), according to the manufacturer's instruction. The RNA samples had RIN values between 8.1 and 8.7. Samples were sequenced at the Norwegian Sequencing Centre (Oslo University Hospital, Ullevål, Oslo). Total RNA samples were subjected to Strand-Specific TruSeqTM mRNA-seq library preparation, and 50 bp paired-end reads were sequenced on an Illumina Novaseq 6000 instrument). To remove/trim low-quality reads and adapter sequences we used BBDuk (BBMap v38.86). Reads were mapped to the Mus musculus reference genome (ENSEMBL release 108) using HiSat2 v.2.1.1[35]. Read counting was done with FeatureCounts v2.0.1[36]. The average read count was 40 million/sample.

Measurement of plasma cholesterol

Plasma cholesterol was measured using colorimetric enzymatic detection kits for detection of total cholesterol (#C75101L, Pointe Scientific, MI, USA) according to manufacturer instructions.

Lipid quantification with HPLC-qTOF/MS

Liver samples (about 100 mg) from 7 to 8 mice in each group were used for lipid analyses using high-performance liquid chromatography (HPLC) coupled to time of flight-mass spectrometry (TOF-MS)[33]. This platform was used to determine separate lipid species such as ceramides (Cer), diacylglycerol (DAG), lysophosphatidylcholine (LPC), phosphatidylcholine (PC), sphingomyelin (SPM), ether-linked phosphatidylcholine (PCO), phosphatidylethanolamine (PE), triacylglycerol (TAG), phosphatidylcholine plasmalogen (PCP), cardiolipins (CL), phosphatidylglycerol (PG), free fatty acids (FFA), hexosylceramides (HexCer), cholesterol (Chol), Cholesteryl esters (CE), lysophosphatidylethanolamine (LPE), and phosphatidylinositol (PI). Detected lipid signals were normalized against liver weights and internal standards. Internal standards used were Cer-35:1, DAG-30:0, LPC-17:1, PC-28:0, SPM-35:1, PE-28:0, TAG 39:0, CL-56:0, PG-30:0, FFA-17:1, HexCer-35:1, Chol-d47, CE19:0, LPE and PI 31:1 (Sigma-Aldrich). The internal standard PC-28:0 was used as a standard for PC, PCO, and PCP.

One sample from *Ubiad1*$^{+/+}$ female was excluded from the analysis due to very deviant lipid values compared to the other 6 *Ubiad1*$^{+/+}$ mice.

Association analysis

Correlations were calculated with the biweight midcorrelation (Bicor) in the HMDP as described[13]. Bicor calculates biweight mid-correlations, which are a robust (less sensitive to outliers) alternative to Pearson correlations. Genotypes for the mouse strains were obtained from Jackson Laboratory using the Mouse Diversity Array[37]. Around 200,000 single nucleotide polymorphisms (SNPs) were left after excluding SNPs with a minor allele frequency of less than 5% and a missing genotype rate of less than 10%. Genome-wide association study (GWAS) for gene expression was performed with FAST-LMM[13], and defined as cis if peak SNP mapped within 1 Mb of gene position (threshold, $p < 6.1 \times 10^{-6}$).

Data analyses

For analyses of RNA sequencing, we used R and integrated Differential Expression and Pathway analysis (iDEP.96), which encompasses many R and Bioconductor packages[38]. Differential expression analyses were done using the DEseq2 pipeline on background filtered read counts. False discovery rate (fdr) < 0.05 and fold change (FC) > 1.5 was considered statistically significant. PCA plots were generated after variance-stabilizing transformation in DEseq2. Enrichment analyses were done using GAGE with GO biological process pathway annotations. For other analyses, we used Graphpad Prism (GraphPad Software, San Diego, CA, USA) software (version 10).

Data availability

The datasets generated and analyzed during the current study are available in the National Center for Biotechnology Information (NCBI) Gene Expression Omnibus (GEO) with accession number GSE266552 and in the article/Supplementary Data. The following secure token has been created to allow review of record GSE266552 while it remains in private status: qtyjiyyuhvivrsx.

Received: 13 May 2024; Accepted: 19 February 2025
Published online: 27 February 2025

References

1. De Pauw, R. et al. Past, present, and future trends of overweight and obesity in Belgium using bayesian age-period-cohort models. *BMC Public. Health.* **22**, 1309. https://doi.org/10.1186/s12889-022-13685-w (2022).
2. Hu, K. & Staiano, A. E. Trends in obesity prevalence among children and adolescents aged 2 to 19 years in the US from 2011 to 2020. *JAMA Pediatr.* **176**, 1037–1039. https://doi.org/10.1001/jamapediatrics.2022.2052 (2022).
3. Ward, Z. J. et al. Projected U.S. State-Level prevalence of adult obesity and severe obesity. *N Engl. J. Med.* **381**, 2440–2450. https://doi.org/10.1056/NEJMsa1909301 (2019).
4. Barsh, G. S., Farooqi, I. S. & O'Rahilly, S. Genetics of body-weight regulation. *Nature* **404**, 644–651. https://doi.org/10.1038/35007519 (2000).
5. Parks, B. W. et al. Genetic control of obesity and gut microbiota composition in response to high-fat, high-sucrose diet in mice. *Cell Metabol.* **17**, 141–152. https://doi.org/10.1016/j.cmet.2012.12.007 (2013).

6. Finucane, M. M. et al. National, regional, and global trends in body-mass index since 1980: systematic analysis of health examination surveys and epidemiological studies with 960 country-years and 9.1 million participants. *Lancet (London England).* **377**, 557–567. https://doi.org/10.1016/S0140-6736(10)62037-5 (2011).
7. Polyzos, S. A., Kountouras, J. & Mantzoros, C. S. Obesity and nonalcoholic fatty liver disease: from pathophysiology to therapeutics. *Metabolism* **92**, 82–97. https://doi.org/10.1016/j.metabol.2018.11.014 (2019).
8. Gerdts, E. & Regitz-Zagrosek, V. Sex differences in cardiometabolic disorders. *Nat. Med.* **25**, 1657–1666. https://doi.org/10.1038/s41591-019-0643-8 (2019).
9. Fazel, Y., Koenig, A. B., Sayiner, M., Goodman, Z. D. & Younossi, Z. M. Epidemiology and natural history of non-alcoholic fatty liver disease. *Metabolism* **65**, 1017–1025. https://doi.org/10.1016/j.metabol.2016.01.012 (2016).
10. Younossi, Z. M. et al. Global epidemiology of nonalcoholic fatty liver disease-Meta-analytic assessment of prevalence, incidence, and outcomes. *Hepatol. (Baltimore Md).* **64**, 73–84. https://doi.org/10.1002/hep.28431 (2016).
11. Lazarus, J. V. et al. NAFLD - sounding the alarm on a silent epidemic. *Nat. Rev. Gastroenterol. Hepatol.* **17**, 377–379. https://doi.org/10.1038/s41575-020-0315-7 (2020).
12. Lovejoy, J. C., Champagne, C. M., de Jonge, L., Xie, H. & Smith, S. R. Increased visceral fat and decreased energy expenditure during the menopausal transition. *Int. J. Obes. (Lond).* **32**, 949–958. https://doi.org/10.1038/ijo.2008.25 (2008).
13. Norheim, F. et al. Gene-by-Sex interactions in mitochondrial functions and Cardio-Metabolic traits. *Cell. Metab.* **29**, 932–949. https://doi.org/10.1016/j.cmet.2018.12.013 (2019). e934.
14. Norheim, F. et al. Genetic and hormonal control of hepatic steatosis in female and male mice. *J. Lipid Res.* **58**, 178–187. https://doi.org/10.1194/jlr.M071522 (2017).
15. Burra, P. et al. Clinical impact of sexual dimorphism in non-alcoholic fatty liver disease (NAFLD) and non-alcoholic steatohepatitis (NASH). *Liver Int.* **41**, 1713–1733. https://doi.org/10.1111/liv.14943 (2021).
16. Shungin, D. et al. New genetic loci link adipose and insulin biology to body fat distribution. *Nature* **518**, 187–196. https://doi.org/10.1038/nature14132 (2015).
17. Jo, Y. & DeBose-Boyd, R. A. Post-Translational regulation of HMG coa reductase. *Cold Spring Harb Perspect. Biol.* https://doi.org/10.1101/cshperspect.a041253 (2022).
18. Mugoni, V. et al. Ubiad1 is an antioxidant enzyme that regulates eNOS activity by CoQ10 synthesis. *Cell* **152**, 504–518. https://doi.org/10.1016/j.cell.2013.01.013 (2013).
19. Hirota, Y. et al. Menadione (vitamin K3) is a catabolic product of oral phylloquinone (vitamin K1) in the intestine and a Circulating precursor of tissue menaquinone-4 (vitamin K2) in rats. *J. Biol. Chem.* **288**, 33071–33080. https://doi.org/10.1074/jbc.M113.477356 (2013).
20. Gaynor, P. M. et al. Accumulation of HDL apolipoproteins accompanies abnormal cholesterol accumulation in Schnyder's corneal dystrophy. *Arterioscler. Thromb. Vasc Biol.* **16**, 992–999. https://doi.org/10.1161/01.atv.16.8.992 (1996).
21. Dong, F. et al. A mouse model of schnyder corneal dystrophy with the N100S point mutation. *Sci. Rep.* **8**, 10219. https://doi.org/10.1038/s41598-018-28545-0 (2018).
22. Jiang, S. Y. et al. Schnyder corneal dystrophy-associated UBIAD1 mutations cause corneal cholesterol accumulation by stabilizing HMG-CoA reductase. *PLoS Genet.* **15**, e1008289. https://doi.org/10.1371/journal.pgen.1008289 (2019).
23. Schumacher, M. M., Jun, D. J., Johnson, B. M. & DeBose-Boyd, R. A. UbiA prenyltransferase domain-containing protein-1 modulates HMG-CoA reductase degradation to coordinate synthesis of sterol and nonsterol isoprenoids. *J. Biol. Chem.* **293**, 312–323. https://doi.org/10.1074/jbc.RA117.000423 (2018).
24. Jo, Y. et al. Enhanced ER-associated degradation of HMG coa reductase causes embryonic lethality associated with Ubiad1 deficiency. *Elife* **9**, e54841. https://doi.org/10.7554/eLife.54841 (2020).
25. Huang da, W., Sherman, B. T. & Lempicki, R. A. Systematic and integrative analysis of large gene lists using DAVID bioinformatics resources. *Nat. Protoc.* **4**, 44–57. https://doi.org/10.1038/nprot.2008.211 (2009).
26. Huang da, W., Sherman, B. T. & Lempicki, R. A. Bioinformatics enrichment tools: paths toward the comprehensive functional analysis of large gene lists. *Nucleic Acids Res.* **37**, 1–13. https://doi.org/10.1093/nar/gkn923 (2009).
27. Schumacher, M. M., Elsabrouty, R., Seemann, J., Jo, Y. & DeBose-Boyd, R. A. The prenyltransferase UBIAD1 is the target of geranylgeraniol in degradation of HMG coa reductase. *Elife* **4**, e05560. https://doi.org/10.7554/eLife.05560 (2015).
28. Shan, T. et al. Adipocyte-specific deletion of mTOR inhibits adipose tissue development and causes insulin resistance in mice. *Diabetologia* **59**, 1995–2004. https://doi.org/10.1007/s00125-016-4006-4 (2016).
29. Norheim, F. et al. Genetic, dietary, and sex-specific regulation of hepatic ceramides and the relationship between hepatic ceramides and IR. *J. Lipid Res.* **59**, 1164–1174. https://doi.org/10.1194/jlr.M081398 (2018).
30. Petersen, M. C. & Shulman, G. I. Roles of diacylglycerols and ceramides in hepatic insulin resistance. *Trends Pharmacol. Sci.* **38**, 649–665. https://doi.org/10.1016/j.tips.2017.04.004 (2017).
31. Jersin, R. A. et al. Role of the neutral amino acid transporter SLC7A10 in adipocyte lipid storage, obesity, and insulin resistance. *Diabetes* **70**, 680–695. https://doi.org/10.2337/db20-0096 (2021).
32. Ran, F. A. et al. Genome engineering using the CRISPR-Cas9 system. *Nat. Protoc.* **8**, 2281–2308. https://doi.org/10.1038/nprot.2013.143 (2013).
33. Li, Y. et al. Plin2 deletion increases cholesteryl ester lipid droplet content and disturbs cholesterol balance in adrenal cortex. *J. Lipid Res.* **62**, 100048. https://doi.org/10.1016/j.jlr.2021.100048 (2021).
34. Doncheva, A. I. et al. Altered hepatic lipid droplet morphology and lipid metabolism in fasted Plin2-null mice. *J. Lipid Res.* **64**, 100461. https://doi.org/10.1016/j.jlr.2023.100461 (2023).
35. Kim, D., Paggi, J. M., Park, C., Bennett, C. & Salzberg, S. L. Graph-based genome alignment and genotyping with HISAT2 and HISAT-genotype. *Nat. Biotechnol.* **37**, 907–915. https://doi.org/10.1038/s41587-019-0201-4 (2019).
36. Liao, Y., Smyth, G. K. & Shi, W. FeatureCounts: an efficient general purpose program for assigning sequence reads to genomic features. *Bioinformatics* **30**, 923–930. https://doi.org/10.1093/bioinformatics/btt656 (2014).
37. Yang, H. et al. A customized and versatile high-density genotyping array for the mouse. *Nat. Methods.* **6**, 663–666. https://doi.org/10.1038/nmeth.1359 (2009).
38. Ge, S. X., Son, E. W. & Yao, R. iDEP: an integrated web application for differential expression and pathway analysis of RNA-Seq data. *BMC Bioinform.* **19**, 534. https://doi.org/10.1186/s12859-018-2486-6 (2018).
39. Mi, H. & Thomas, P. PANTHER pathway: an ontology-based pathway database coupled with data analysis tools. *Methods Mol. Biol.* **563**, 123–140. https://doi.org/10.1007/978-1-60761-175-2_7 (2009).

Acknowledgements

This research was supported by FY 2022 Researcher Exchange Program between Japan Society for the Promotion of Science and the Research Council of Norway, the Norwegian Diabetes Association, The Nansen Foundation, Frimed Foundation, and The Johan Throne Holst Foundation.

Author contributions

Conceptualization, F.A.N. and R.H.; Data curation, F.A.N., C.P., S.N.D., M.M.S., K.T.D and R.H.; Formal Analysis, R.H., P.K., S.N.D., M.M.S., C.P., and F.A.N.; Funding acquisition, F.A.N., R.H.; Investigation, R.H., S.P.,

P.K., K.T.D and F.N.; Methodology, F.N., C.P., R.H.; Project administration, R.H. and F.A.N.; Recourses, F.N., K.T.D., S.N.D., J.F., G.M. and A.J.L.; Supervision, F.N., C.A.D., and K.T.D.; Validation, R.H. and S.P.; Visualization, R.H. and F.A.N.; Writing—original draft preparation, R.H. and F.A.N.; Writing—review and editing, R.H., S.P., K.T.D., S.N.D., C.A.D, J.F., G.M., A.J.L., and F.A.N; All authors have read and agreed to the published version of the manuscript.

Declarations

Competing interests
The authors declare no competing interests.

Additional information
Supplementary Information The online version contains supplementary material available at https://doi.org/10.1038/s41598-025-91283-7.

Correspondence and requests for materials should be addressed to F.A.N.

Reprints and permissions information is available at www.nature.com/reprints.

Publisher's note Springer Nature remains neutral with regard to jurisdictional claims in published maps and institutional affiliations.